JOURNAL OF COMPUTATIONAL PHYSICS **126,** 139–151 (1996)
ARTICLE NO. 0126

Coupling of Two Absorbing Boundary Conditions for 2D Time-Domain Simulations of Free Surface Gravity Waves

A. CLÉMENT

Laboratoire de Mécanique des Fluides, CNRS URA 1217 E.C.N., 1 Rue de la Noe, 44300 Nantes, France

Received January 3, 1995; revised November 8, 1995

The numerical simulation of nonlinear gravity waves propagating at the surface of a perfect fluid is now usually solved by totally nonlinear time-domain numerical models in two dimensions, and this approach is being extended to three dimensions. The original initial boundary value problem is posed in an unbounded region, extending horizontally up to infinity to model the sea. Its numerical solution requires truncating the domain at a finite distance. Unfortunately, no exact nonreflecting boundary condition on the truncating surface exists in this time-domain formulation. The proposed strategy is based on the coupling of two previously known methods in order to benefit from their different, and complementary, bandwidth: the numerical ''beach,'' very efficient in the high frequency range; and a piston-like Neumann condition, asymptotically ideal for low frequencies. The coupling method gives excellent results in the whole range of frequencies of interest and is as easy to implement in nonlinear as in linear versions. One of its major advantages is that it does not require any spectral knowledge of the incident waves.

INTRODUCTION

A large number of numerical methods devoted to the simulation of two-dimensional nonlinear free surface flows appeared in the literature during the last decade. Most of them are based on the so-called mixed Euler–Lagrange (MEL) approach introduced in 1976 by Longuet-Higgins and Cokelet [1]. A lot of different applications, including strongly nonlinear problems which could not be solved before became amenable to numerical simulation, up to the limit of the wave breaking occurrence. All these time-domain models are based on time stepping; they require the solution of a boundary value problem for the velocity potential at every time step. Their application to open domain problems like those encountered in naval applications requires the artificial truncation of the domain with a fictitious surface where a nonreflecting boundary condition (NRBC) must be introduced in order to let the waves exit the domain as they would do in the open sea.

This is a common problem in numerical modelling of wave propagation in many fields of physics. An extensive review of NRBCs for phenomena driven by the wave equation may be found in Givoli [2].

For this kind of equations in unbounded domains, exact absorbing boundary conditions nonlocal in both space and time [3], or partially nonlocal [4, 5] has been developed for FEM solvers. Following Engquist and Majda [6], some authors have devised higher order approximate local NRBC, in order to improve the results obtained with the classical first-order Sommerfeld condition [7–9]. Using similar techniques, Bayliss *et al.* [10] derived high order NRBC for time independent elliptic problems in exterior region.

The mathematical modelling of the propagation of free surface gravity waves leads to an initial boundary value problem (IBVP) posed in a domain bounded by a moving unknown free surface on which a nonlinear boundary condition has to be satisfied. In that context, even after linearizing that condition which leads to posing the problem in a fixed time independent domain, no exact absorbing condition preventing spurious reflection exists on the fictitious closure boundary we are obliged to introduce closing the domain at a finite distance. Thus, the absorption of outgoing waves in the numerical simulation of unsteady free surface hydrodynamics is still an open problem.

A well-known solution (see, e.g., [11–13]) consists in matching the inner solution at the truncation boundary with an outer one generated by Kelvin's Green function which satisfies intrinsically the free surface condition. These Green functions relative to free surface hydrodynamics were formulated a long time ago [14] in either frequency or time-domain linear formulation. But, being basically limited to linear application, they impose matching at a large distance in order to minimise the difference between the inner nonlinear solution and the linear outer one and, consequently, increasing the size of the computational domain.

Using Rankine's Green functions to solve the inner problem allows the solution of linear, as well as nonlinear formulations of water wave propagation problems. As a

0021-9991/96 $18.00

counterpart, this approach necessitates truncating the computational domain at a finite distance and absorbing outgoing waves at the artificial end of the domain by a strategy fitted to and included in the IBVP solver. A thorough review of the available numerical techniques to solve this problem may be found in Romate [15].

In the frequency domain, the well-known Sommerfeld condition provides a simple linear relation between the partial time derivative (i.e., the dynamic pressure) and the normal derivative (i.e., the horizontal fluid velocity). Unfortunately, this condition has no counterpart in the time domain. The so-called Orlanski's condition [16], used by a lot of authors (see, e.g., [17–20]), is nothing but a simple transposition of the Sommerfeld relation to the time domain, replacing the frequency dependent wave phase velocity by a time varying "velocity-like" coefficient $c(t)$. This condition is local in both time and space and cannot therefore give good results for purely unsteady (i.e., nonmonochromatic) incident waves. It is easy to show, indeed, that an exact absorbing condition for free surface waves should be nonlocal at least in time to account for the dispersive nature of the free-surface condition. Thus, the use of the Orlanski condition should be restricted to the cases of regular incident waves of known frequency, or to very long waves, because in both cases the velocity coefficient is actually a constant after the transient phase of the flow from rest.

This feature does not fit the aim of our study which was primarily to devise an absorption strategy that is independent of the spectral content of the incident wave train and efficient even in transient and purely unsteady free surface flows.

In Section 2, we present the absorption performances of a piston-like absorbing boundary condition (PABC) derived from the study of an experimental wave-absorber device for wave tanks [25, 26]. In the present application to numerical wave basins, the piston control law was simplified in order to retain only the low frequency asymptotic term. As a consequence, this boundary condition is efficient only in the small frequency range, but we shall see that this drawback will be easily compensated by the coupling.

An alternative method (see [21–24]) consists in introducing an extra dissipative term in the free surface condition on a limited portion of this surface adjacent to the artificial boundary (see Fig. 1). Passing through this area, waves lose a part of their energy first on their way out and then, for that part reflected upon the boundary, on their way back. This method is sometimes referred to as the "numerical beach" method. It may be very efficient for high frequency waves, provided the beach length is longer than the typical wavelength of incident waves. This method is presented in Section 3.

Comparing the performance curves (i.e., efficiency versus frequency) of these two methods clearly highlights their complementarity in terms of bandwidth and naturally led us to experiment their coupling. As we shall see in Section 4, the results obtained by this coupling were found to be excellent, better in fact than we expected and as good in linear as in nonlinear simulations.

Compared to the previous methods ("absorbing beach," Orlanski's condition, ...), the major advantage of this new coupling method is that it ensures high absorption efficiency whatever the spectral content of the incident waves may be (regular, bichromatic, narrow or wide banded irregular, solitary waves), and without any kind of tuning with respect to their frequency. This kind of robustness is crucial when developing a general purpose numerical wave basin.

1. NUMERICAL SIMULATION OF 2D FREE SURFACE GRAVITY WAVES

The initial boundary value problem to be solved is derived through the usual assumptions of the free-surface potential flow theory; i.e., the fluid is incompressible and inviscid, surface tension is not considered, the atmospheric pressure is constant in both space and time and is given a null reference value, and the flow is irrotational. The free-surface flow is driven by gravity only. The fluid velocity is thus the gradient of a scalar potential function Φ of space and time: $\mathbf{V}(M, t) = \nabla\Phi(M, t)$.

The fluid domain $\mathscr{D}$ is bounded by (Fig. 1):

—the free surface $\mathscr{F}$

—the bottom $\mathscr{B}$

—the wave making surface $\mathscr{C}$

—the wave absorbing surface $\mathscr{P}$.

The free surface $\mathscr{F}$ is a function of time and is unknown a priori. $\mathscr{F}_d$ denotes a portion of $\mathscr{F}$ on which a modification of the free surface condition will be introduced. In order to save computing time, particularly in nonlinear simulations, the water depth was taken constant in the present study, but the method would apply to uneven bottoms as well, without expected loss of efficiency, provided the distance between the bottom irregularity and the absorbing zone is large enough. It has been used with success in the case of the diffraction of a solitary wave by a circular cylinder sitting on the bottom. In the present framework of free-surface potential flows, a nonuniform bottom would simply diffract the water waves propagating in the domain without changing their nature with regard to the proposed absorption method.

The left end of the domain $\mathscr{C}$ will be given a prescribed motion to generate gravity waves which will propagate from this wave making surface in the x-positive direction. The right end of the fluid domain consists of a vertical surface $\mathscr{P}$. The goal of the present method is to prevent wave reflection upon this termination as if the domain

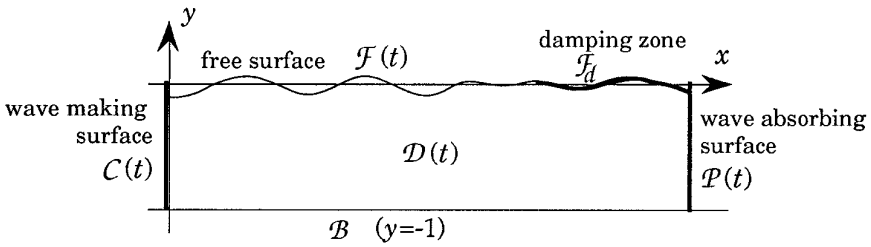

FIG. 1. The two-dimensional fluid domain.

was unbounded, by a suitable combination of boundary conditions on $\mathscr{P}$ and $\mathscr{F}$. On $\mathscr{P}$, a time variable Neumann condition will define the motion of this surface in response to the incident wave train.

As can be noticed, all the boundaries of the problem are moving surfaces, except the bottom. Furthermore, the motion and the position of the free surface and of the wave absorbing surface are themselves unknowns of the problem.

1.1. *The Potential Initial-Boundary-Value Problem (IBVP)*

Under the above assumptions, the velocity potential must satisfy the set of conditions

$$\nabla^2\Phi(M,t) = 0, \qquad M \in \mathscr{D}, t \geq 0, \tag{1.1}$$

$$\frac{D\mathbf{x}}{Dt} = \nabla\Phi, \qquad M \in \mathscr{F}, t \geq 0, \tag{1.2}$$

$$\frac{D\Phi}{Dt} = -y + \tfrac{1}{2}(\nabla\Phi)^2, \qquad M \in \mathscr{F}, t \geq 0, \tag{1.3}$$

$$\frac{\partial\Phi}{\partial x}(y,t) = \frac{dx}{dt} = w(t), \quad M \in \mathscr{C}, t \geq 0, \tag{1.4}$$

$$\frac{\partial\Phi}{\partial y} = 0, \qquad M \in \mathscr{B}, t \geq 0, \tag{1.5}$$

where D/Dt denotes the Lagrangian material derivative. w is a given function of time only; then $\mathscr{C}$ is a numerical piston wavemaker.

The gravity acceleration g was set to unity and the water depth h was chosen as the reference to nondimensionalize the length variables of the problem. This introduces the natural reference value $(h/g)^{1/2}$ for all the time variables which will thus be nondimensionalized with respect to it from now on in the whole paper.

The choice of a *piston-like* Neumann condition as (1.4) on the opposite wave absorbing surface $\mathscr{P}$ is motivated by asymptotic properties of the transient incident waves to be absorbed and will be discussed later (see Section 3). At the moment, let us just give it the same general form as (1.4):

$$\frac{\partial\Phi}{\partial x}(y,t) = \frac{dx}{dt} = v(t), \quad M \in \mathscr{P}, t \geq 0. \tag{1.6}$$

The set of equations (1.1) to (1.6) forms an initial-boundary-value problem for the velocity potential Φ. Provided that initial conditions are known on the free surface and that the function $v(t)$ and $w(t)$ are given from $t = 0$ up to the current time value t, this problem may be solved by the time marching procedure briefly described in Section 1.3.

1.2. *The Associated Dynamic Pressure IBV Problem*

Let us now define the dynamic pressure Ψ by

$$\Psi(M,t) = \frac{\partial\Phi}{\partial t}(M,t).$$

The total pressure at any point M in the fluid domain is given by the Bernoulli equation,

$$p(M,t) = -y - \Psi - \tfrac{1}{2}(\nabla\Phi)^2 \tag{1.7}$$

and the resulting hydrodynamic force on any solid body is obtained by integrating the pressure along its wetted surface $\mathscr{S}$:

$$\mathbf{F}(t) = \int_{\mathscr{S}} p\mathbf{n}\, ds. \tag{1.8}$$

When $\mathscr{S}$ is fixed, or is given a prescribed motion, the calculation of $\mathbf{F}$ can be achieved as a postprocessing task, computing the time derivative Ψ by a finite difference scheme from the results of the Φ problem. But suppose now $\mathscr{S}$ to be moving in response to the waves, then the problems in Φ and Ψ are coupled and must be solved simultaneously to permit the integration of the ordinary differential equations (1.4), (1.6) giving access to the instantaneous boundary position. Two strategies may be adopted to handle this problem:

—the partial time derivative Ψ may be evaluated by a finite difference scheme [19, 29, 30].

—a parallel initial boundary value problem may be

solved for Ψ (see, e.g., Vinge *et al.* [31], Cointe [23, 24], Jagannathan [18]).

The latter method was preferred here mainly due to the fact that it requires practically no extra numerical cost, simply adding one supplementary RHS to the linear system already built to solve for Φ by a BEM method.

The Ψ problem is posed as

$$\left.\begin{aligned} \nabla^2\Psi(M,t) &= 0, && M\in\mathscr{D}\\ \Psi &= -y-\tfrac{1}{2}(\nabla\Phi)^2, && M\in\mathscr{F}\\ \frac{\partial\Psi}{\partial x}(y,t) &= \left[\dot w(t)-w(t)\frac{\partial^2\Phi}{\partial y^2}\right], && M\in\mathscr{C}\\ \frac{\partial\Psi}{\partial x}(y,t) &= \left[\dot v(t)+v(t)\frac{\partial^2\Phi}{\partial y^2}\right], && M\in\mathscr{P}\\ \frac{\partial\Psi}{\partial y} &= 0, && M\in\mathscr{B} \end{aligned}\right\}, \quad t\ge 0, \quad (1.9)$$

where the overdot denotes differentiation with respect to time. The boundaries positions are updated by the ODEs integration in the parallel solution of the Φ problem.

Under the assumptions of small wave steepness and small displacements of the solid boundaries from their initial rest position, the above nonlinear IBVPs for Φ and Ψ may be linearized and posed in a fixed geometrical domain $\mathscr{D}$. In that case, the LHS of the linear system to be solved becomes time invariant and the matrix may be assembled and possibly preconditioned or inverted, once and for all at the beginning of the computation.

The proposed method for outgoing wave absorption was implemented and tested in both linear and nonlinear versions of the algorithm.

1.3. *The Time-Stepping Solution of* Φ *and* Ψ *Problems*

Suppose the ODEs (1.2), (1.3) have been solved up to the time $t_k = k\delta$, where k is a positive integer and δ is the time step. At this instant t_k, the geometry of the domain in which Laplace's equation applies, the normal velocity Φ_n on the material surfaces $\mathscr{C}$, $\mathscr{P}$, and $\mathscr{B}$, and the potential Φ itself on the free surface $\mathscr{F}$ are known.

This mixed Neumann–Dirichlet boundary-value-problem may be solved by a boundary element method (BEM), as is generally the case for this kind of nonlinear simulation of free surface potential flows. Because emphasis will be put on the outgoing wave absorption in this paper, we shall just recall hereafter the main features of our algorithm ([27]):

—plane panels are used to approximate the domain boundary,

—the strength of Rankine sources and dipoles varies linearly on the panels,

—mirror image singularities with respect to the plane bottom are used in order to eliminate the discretization of this surface,

—the evolution of the vertices is Lagrangian on the free surface, and Eulerian on the material surfaces,

—a double node technique is used at the intersection of the free surface with the vertical boundaries,

—the solid body surfaces are regridded every time step with a length constraint at the intersection with the free-surface, in order to optimize the solution accuracy at the corner.

Once the BVP problem for Φ has been solved that way at $t = t_k$, both the potential and its normal derivative are known on all the domain boundaries. Then, the boundaries' geometry can be advanced in time to t_{k+1} by integrating the ODEs (1.2), (1.4), (1.6), and the Dirichlet condition is updated on the free surface integrating (1.3) by a standard fourth-order Runge–Kutta procedure, including an in-line dynamic time step adaptation. The tangential velocity $\partial\Phi/\partial s$ needed in the evaluation of the right-hand side of (1.3) is calculated by a weighted arctang method [28],

$$\frac{\partial\Phi}{\partial s}(s_i) = \tan\left[\frac{\theta_i(s_i - s_{i-1}) + \theta_{i-1}(s_{i+1} - s_i)}{(s_{i+1} - s_{i-1})}\right], \quad (1.10a)$$

where

$$\theta_i = \tan^{-1}\left[\frac{\Phi_{i+1} - \Phi_i}{s_{i+1} - s_i}\right]. \quad (1.10b)$$

The new geometry of the domain and the updated Neumann and Dirichlet boundary conditions being known at the new time step t_{k+1}, the process may be iterated.

We must emphasize here that this implementation of the MEL method was found exempt from any sawtooth instabilities of the free surface reported by several authors and that, consequently, neither regridding nor smoothing of the free surface were necessary in the numerous nonlinear simulations performed with this code.

2. THE PISTON-LIKE ABSORBING BOUNDARY CONDITION (PABC)

The Neumann boundary condition (1.6) is said to be *piston-like* because the horizontal velocity $v(t)$ is not local in space, i.e. v is not a function of y. This is a fundamental difference with the widely used Orlanski condition,

$$\frac{\partial\Phi}{\partial x}(y,t) = \frac{1}{c(t)}\frac{\partial\Phi}{\partial t}(y,t), \quad (2.1)$$

where the local normal velocity is considered to be proportional to the dynamic pressure and, therefore, a function of y. This condition is nothing but a direct transposition in the time domain of the Sommerfeld condition which is asymptotically exact in the frequency domain as the absorbing boundary is moved far away from the wave source. In that specific case of time harmonic flow, the coefficient c in the absorbing boundary condition is actually the phase velocity of the incident waves and is a real function of the wave frequency ω. Then the transposition of the Sommerfeld condition to the time domain should formally be obtained by the inverse Fourier transform and should result in a convolution product which implies a relation nonlocal in time between the normal derivative and the dynamic pressure, instead of a form like (2.1). The coefficient $c(t)$ in this relation has the dimension of a velocity but is void of any physical meaning and cannot be derived from the known solution of the problem in the frequency domain.

In some reported numerical applications of the Orlanski condition (2.1), this coefficient is kept constant and equal to the upper limit value $\sqrt{gh}$ of the long wave velocity in the linear theory of free surface waves; but in most cases, it is considered as an actual function of time and continuously extrapolated from the results of previous time steps during the simulation (see, e.g., [17, 18]). This in-line estimation requires the knowledge of the potential in the fluid domain, in the vicinity of the absorbing boundary $\mathscr{P}$. When the problem is solved by finite differences [37] or FEM [17], this is easy to implement, but in a BEM context, where solutions are known only on the boundaries, this feature makes the Orlanski condition more difficult to implement [18, 38].

2.1. *Principle and Derivation*

The piston-like condition proposed here is very easy to implement, especially when solving by BEM, either in linear or nonlinear formulation. It derives from results obtained in the study of the control of physical wave absorbing devices for wave tanks [25, 26].

Let $f(t)$ denote the horizontal component of the hydrodynamic force on the piston $\mathscr{P}$, excluding the hydrostatic term, obtained by integrating the pressure along its wetted surface. Hence,

$$f(t) = \int_{\mathscr{P}(t)} \left[-\frac{\partial \Phi}{\partial t} - \tfrac{1}{2}(\nabla \Phi)^2 \right] dl. \tag{2.2}$$

Given this force signal from the initial state of rest at $t = 0$ up to the present time t, the optimal control problem was to find the piston ideal velocity law: $\tilde{v}(t)$, leading to 100% wave absorption when used as the RHS of the Neumann boundary condition (1.6). Milgram [32] tried to solve the same problem driving, not a piston, but a hinged plate from the wave elevation signal, instead of the force signal.

The solution of this control problem is straightforward in the linearized frequency domain formulation of the problem. Denoting by ω the circular frequency, and writing

$$\begin{aligned} f(t) &= \Re_e\{F(i\omega)e^{i\omega t}\} \\ v(t) &= \Re_e\{V(i\omega)e^{i\omega t}\}, \end{aligned} \tag{2.3}$$

it can be shown [25] that the transfer function between the *ideal* velocity and the force is given by

$$\frac{\tilde{V}(i\omega)}{F(i\omega)} = H(i\omega) = \tfrac{1}{2}\left[\frac{\omega^5}{m_0^3(\omega^2 - \omega^4 + m_0^2)} + i\omega \sum_{k=1}^{\infty} \frac{\omega^4}{m_k^3(\omega^2 - \omega^4 - m_k^2)} \right]^{-1}, \tag{2.4}$$

where $m_0 \tanh m_0 = \omega^2$ and $m_k \tanh m_k = -\omega^2$, and the tilde denotes the values of the variables in the *optimal* (i.e., perfectly absorbing) regime.

In this linear formulation of the problem, (2.4) may easily be transposed to the time domain through the convolution theorem, leading to

$$\tilde{v}(t) = \int_{-\infty}^{\infty} f(\tau) h(t - \tau)\, d\tau \tag{2.5}$$

in which $h(t)$ is the inverse Fourier transform of $H(i\omega)$. Thus, the instantaneous velocity of the *perfect* piston wave absorber is formally given by the convolution product (2.5) of the hydrodynamic force by $h(t)$. The lower bound of this integral can be set at the instant when the fluid starts from rest, which may be chosen as the origin of the time variable. But, due to the fact that $h(t)$ is *anticausal* [25, 33], that is, ($h(t) = 0$ for $t > 0$ and $h(t) \neq 0$ for $t < 0$), the upper bound must be extended up to ∞. Thus the computation of (2.5) which would require the knowledge of the future values of the force is clearly not realizable. For physical applications of (2.5) to the water wave absorbing device control, we have developed nonoptimal feedback–feedforward control strategies from realizable approximations of $H(i\omega)$ [25, 26].

In the present numerical extension of that work, we shall focus only on the low frequency asymptotic behaviour of $H(i\omega)$. In the limit $\omega \to 0$, the modulus of the transfer function tends to 1, while the phase remains negligible up to $\omega \cong 1$ (see Fig. 2). Thus, when $\omega \to 0$, the relation (2.4) simply becomes at the leading order

$$\tilde{V}(i\omega) = F(i\omega), \tag{2.6}$$

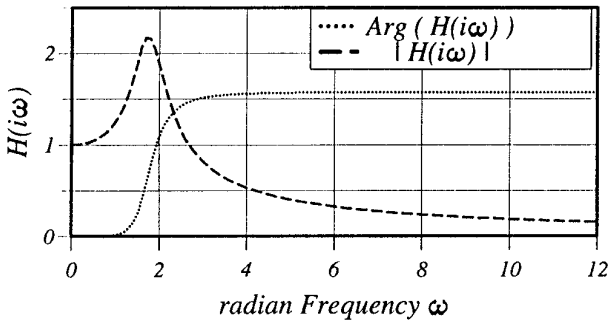

FIG. 2. Frequency domain transfer function $H(i\omega)$ of the ideal piston wave absorber.

resulting, in the time domain, in the boundary condition on the control surface $\mathscr{P}$,

$$\frac{\partial \Phi}{\partial x} = \int_{\mathscr{P}(t)} \left[-\frac{\partial \Phi}{\partial t} \right] dl, \quad M \in \mathscr{P}, t \geq 0, \tag{2.7}$$

which will be denoted as the piston-like absorbing boundary condition (PABC) in the following. Due to the validity range of this approximation, the corresponding absorption strategy was expected to give its best results in the low frequency range. In order to check this point, it was first implemented and tested in the linear version of the numerical basin and then in the general nonlinear code (Sections 1.1 to 1.3). Results for both applications are given in Section 2.3 below.

2.2. *Numerical Estimation of the Absorption Efficiency*

There are several ways by which the performance of a wave absorbing technique in the time domain may be quantified. In the present study we used one of the two following methods, depending on the nature of the incident waves.

For monochromatic wave packets generated by the left vertical surface $\mathscr{C}$ acting as a wavemaker, we proceeded by measuring the decrease in amplitude before and then after their partial reflection/absorption at the opposite absorbing end (cf. Fig. 3). Let A_0 denote the amplitude of the incident wave packet, and A_1 its amplitude after the first reflection. An amplitude absorption coefficient may then be defined by

$$C_A = 1 - \frac{A_1}{A_0}. \tag{2.8}$$

Another way to proceed is to evaluate the energy decay during the absorption. Let E_0 be the initial amount of energy brought to the fluid by the wavemaker, and E_1 the energy level after the absorption of the wave train. An energy absorption coefficient may be defined the same way as above, but now from the energy decay:

$$C_E = 1 - \frac{E_1}{E_0}. \tag{2.9}$$

This second method was used whenever the former one was not appropriate, as for instance when testing absorption of bichromatic wave trains (see Section 4.2).

For steady state monochromatic waves, the two coefficients should verify:

$$(1 - C_E) = (1 - C_A)^2. \tag{2.10}$$

The quality of the IBVP solver with regard to energy conservation was incidentally checked by the close satisfaction of (2.10) we noticed in the computations reported in Section 4.1, although the flow was not a steady state but a transient one.

2.3. *Efficiency versus Frequency*

As stated above, the PABC (2.7) was first implemented in the linear code and then in the nonlinear numerical wave basin.

The amplitude absorption coefficient C_A was determined by the first method mentioned above for nondimensional wave frequencies in the range $\omega \in]0, 3]$ which amply covers the range of practical interest.

Results are plotted on Fig. 4 for both linear and nonlinear applications. In linear simulations, the wavemaker amplitude was set up in such a way that its stroke remains negligible regarding the basin length (ratio = $O(10^{-3})$). In nonlinear computations, the same criterion was applied, combined with a fixed value of the wave steepness γ which is the intrinsic parameter in the linearization of the free surface boundary conditions (1.2), (1.3). The steepness is defined as the ratio of the wave height over the wavelength. The theoretical upper limit of this parameter before wave breaking is 0.14. All the nonlinear simulations reported herein were performed with $\gamma \cong 0.05$, except in Section 4.1, where γ was varied to study its influence on the absorption efficiency.

This behaviour of the absorption coefficient with respect to the frequency is not surprising if we remember that the boundary condition (2.7) is asymptotically an ideal time-domain wave absorber when $\omega \to 0$. The coefficient tends to 1 in that limit and decreases rapidly after $\omega = 1$, as was anticipated from the comments about Fig. 2 in Section 2.1. This absorption device then behaves like a *high-pass* filter with regard to the incoming water waves.

The most remarkable feature of these results lies in the very tiny difference between the linear and the nonlinear codes. This was expected from the heuristic point of view,

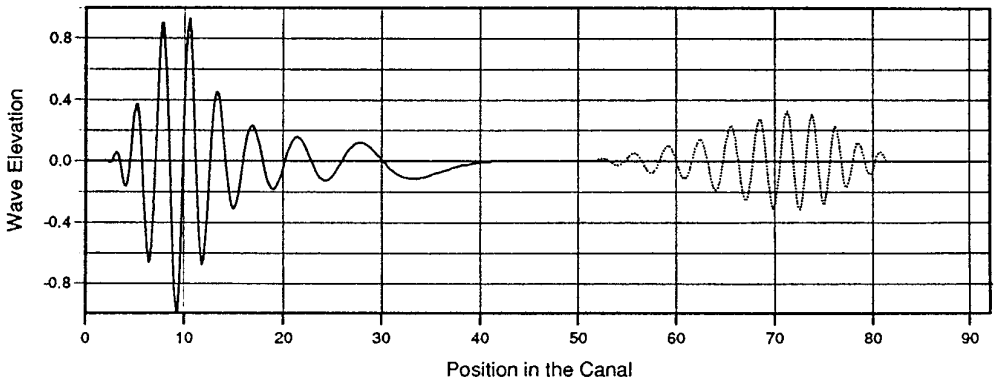

FIG. 3. Right-going incident wave packet (solid) and its left-going reflected part (dotted).

but it remained to be confirmed by numerical experiments. This made us confident in the applicability of the coupling, in the nonlinear time-domain simulations, to the beach method we shall introduce in the next section.

Before that, a point must be cleared up about the practical implementation of the PABC (2.7) in *nonlinear* codes. In that context, the question of including or not the quadratic terms of (2.2) in the RHS of (2.7) was left open. Both options were implemented and tested, and we have noticed that including, or not, these terms in the PABC results in negligible difference in the wave absorption efficiency.

The contribution of these terms to the global hydrodynamic force is usually referred to as *slowly varying* forces. As a matter of fact, given an incident wave spectrum, the quadratic nature of this pressure term results in low-frequency and high-frequency force components. The effects of the latter are generally negligible due to the very low energy level they carry. On the other hand, the low-frequency forces are responsible for the slow horizontal drift motion of floating bodies. In the present case, taking this term into account in the PABC would result in the same kind of phenomena due to the time integration of the piston velocity during the simulation. The consequence would be a slow drift of the end wall of the basin which should result in a global decrease of the mean water level. We consequently recommend not including the quadratic term and still using (2.7), even in the nonlinear implementation of the method.

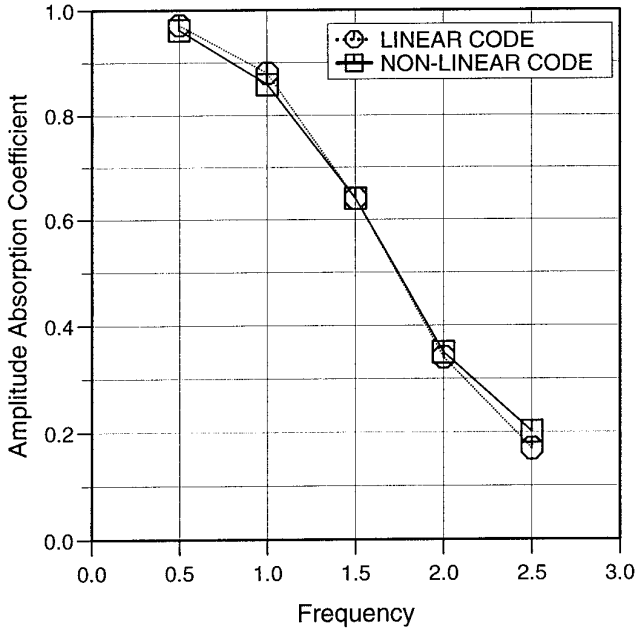

FIG. 4. Absorption coefficients of the piston-like boundary condition versus incident wave frequency.

3. THE "NUMERICAL BEACH" METHOD

This method was first used by Baker *et al.* [22] in the numerical solution of a similar 2D water wave problem. The idea, from Israeli and Orszag [21] is quite simple. It consists in adding to the dynamic free surface condition (1.3), or to the kinematic condition (1.2), or both, an extra dissipative term in a limited area of the free surface $\mathscr{F}_d$, adjacent to $\mathscr{P}$(see Fig. 1). Thus, passing through this damping zone in whatever direction of propagation, the water waves progressively lose their energy. Provided the damping zone is sufficiently long with regard to the wavelength and the dissipation is sufficiently efficient, the waves may be entirely absorbed. This method is sometimes referred to as a "sponge layer" [15, 21], or a "numerical beach" [24]. We shall use the latter one for convenience in the following.

After incorporating these new dissipative terms, the general form of the modified free surface conditions (1.2), (1.3) becomes

$$\left.\begin{aligned} \frac{D\Phi}{Dt} &= -y + \tfrac{1}{2}(\nabla\Phi)^2 - \nu(x)F \\ \frac{D\mathbf{x}}{Dt} &= \nabla\Phi - \mu(x)X \end{aligned}\right\}, \quad M \in \mathscr{F}_d. \qquad (3.1)$$

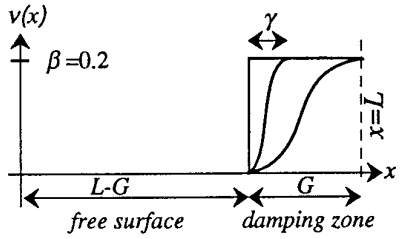

FIG. 5. $\nu(x)$ for $\gamma/G = 0.$, $\gamma/G = 0.25$, and $\gamma/G = 1$.

The nature of the added dissipative terms is arbitrary, and a variety of solutions can be found in the related literature. F and X may be chosen as functions of potential, particle velocity, wave elevation, or any combination of them, or whatever. Some authors modify only the kinematic condition and leave the dynamic condition unchanged (i.e., $F = 0$), while others made the opposite choice [34]. Following Baker *et al.* [22], Telste [35], and Cointe [23, 24] implemented simultaneously both modified conditions.

All these methods are potentially very efficient, but their efficiency strongly depends on the ratio between the beach length and the wavelength. The longer the wavelength is, the longer the length of the beach must be to reach a given absorption level [23]. This feature is clearly illustrated by the secondary G/λ scale we plotted at the top of Fig. 6. Thus, this kind of absorbing method will naturally behave as a *low-pass* filter for the incident water waves, the cutoff frequency of which must be tuned to the spectral content of the incoming waves in order to maintain good absorption performances for the longer waves. We shall see in Section 4 that this requirement is naturally cancelled by coupling with the PABC *high-pass* filter.

Several variants of the added dissipative term have been tested, and we finally retained, in both linear and nonlinear simulations, the following modified free surface boundary conditions:

$$\left.\begin{aligned} \frac{D\Phi}{Dt} &= -y + \tfrac{1}{2}(\nabla\Phi)^2 - \nu(x)\,\frac{\partial\Phi}{\partial n} \\ \frac{D\mathbf{x}}{Dt} &= \nabla\Phi \end{aligned}\right\}, \quad M \in \mathscr{T}_d. \qquad (3.2)$$

Our choice of a function F proportional to Φ_n in (3.2) ensures the energy flux to be always positive from the fluid domain to the exterior domain (i.e., the added term is always dissipative [32]).

The matching between the free-surface and the "beach" must be smooth enough in order to avoid partial reflection when the waves enter the damping zone. Several $\nu(x)$ have been tested. We finally defined a function $\nu(x)$ which is made of three parts (Fig. 5). It is null for x less than $(x_{\max} - G)$; G being the beach length, it is equal to its final step value β near the end wall, and it is defined as a cubic polynomial in the transition zone of length γ. Figure 6 shows the sensitivity of the beach efficiency with respect to the "smoothness" of the transition; this is particularly highlighted by the solid curve corresponding to a beach with a step $\nu(x)$ function upon which short waves ($\lambda < 1.4G$) reflect more and more as their wavelength decreases.

The numerical optimization of the parameters β and γ was achieved using the linear version of the code, and we finally retained $\beta = 0.2$ and $\gamma = G$.

As mentioned earlier, our primary goal was to devise a time-domain numerical method of water wave absorption working *blindly* with regard to the incoming waves and needing no kind of previous or in-line tuning. According to this constraint, the beach length was kept constant ($G = 2$), that is, twice the water depth, in all the tests reported herein.

4. COUPLING THE "BEACH" AND THE "PISTON"

The PABC method being efficient for low frequencies and the beach, for high frequencies, the idea of coupling them, originally suggested by Israeli *et al.* [21] for a one-dimensional wave equation, came very naturally. Both of them were then implemented in our numerical 2D wave basin (CANAL-1.2) to evaluate the performances of the coupling. This implementation is numerically straightfor-

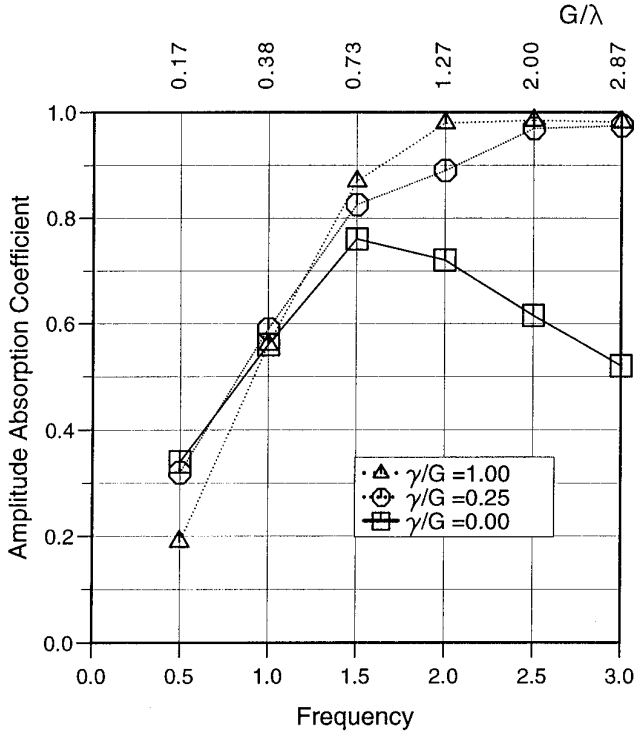

FIG. 6. Numerical beach absorption coefficient.

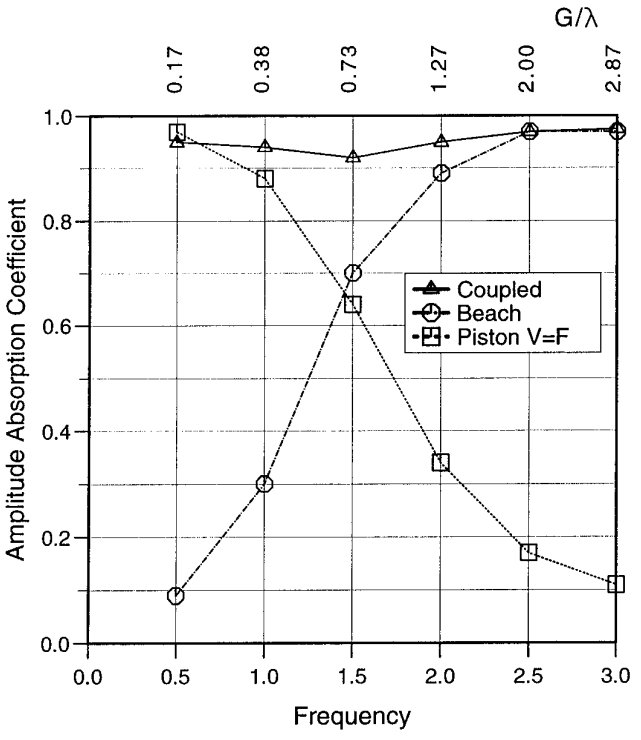

FIG. 7. Coupled Piston + Beach methods implemented in the *linear* IBVP solver.

ward. The PABC is nothing but the response of a body to wave excitation, a problem which was already handled in the original code for floating bodies; on the other hand, adding the dissipative term in the free surface condition introduces no extra unknown to the problem, thus practically no extra computational burden.

4.1. *Absorption of Monochromatic Wave Packets in the Time Domain*

In order to compare with the results obtained by using each method separately, the coupling method was tested with the same set of monochromatic incident wave packets as described in Section 2.2.

The results are shown by the dotted lines with triangles on Fig. 7 for the linear application and on Fig. 8 for the nonlinear case. The global behaviour of the absorption coefficient versus the incoming wave frequency conforms to our expectations. The coupling benefits from the behaviour of both methods in the medium frequency range. In the worst case ($\omega \approx 1.5$), where neither the numerical beach nor the piston boundary conditions used alone were able to absorb more than 70%, the coupling results in an absorption coefficient never smaller than 0.93 (in terms of amplitude ratios, that is, 0.995 for the corresponding absorption coefficient in energy).

Another very interesting feature of these results appears on Figs. 7 and 8, where we can see indeed that the method works as efficiently in linear as in nonlinear implementations.

As mentioned in Section 2.3, the nonlinear simulations reported on Fig. 8 were performed with a constant wave steepness γ of approximately 5%. In order to check the sensitivity of the method with regard to this parameter in nonlinear applications, we made additional simulations with monochromatic wave packets, keeping constant the frequency at ($\omega \approx 1.5$), where the absorption coefficient is minimum, but varying the wave amplitude from very low steepness waves ($\gamma \cong 0.01$) up to quite breaking waves ($\gamma \cong 0.10$).

The results plotted on Fig. 9 show that the coupling method is more and more efficient as the wave height increases, the coefficient growing up more than linearly with the steepness. This behaviour is very encouraging for using the coupling method in numerical simulations of highly nonlinear water waves.

4.2. *Absorption of Bichromatic Waves*

All the tests reported in the above section 4.1 were performed with monochromatic waves. The question of multifrequency incident wave trains had then to be examined before concluding about the applicability of the method in the time domain for any kind of outgoing waves.

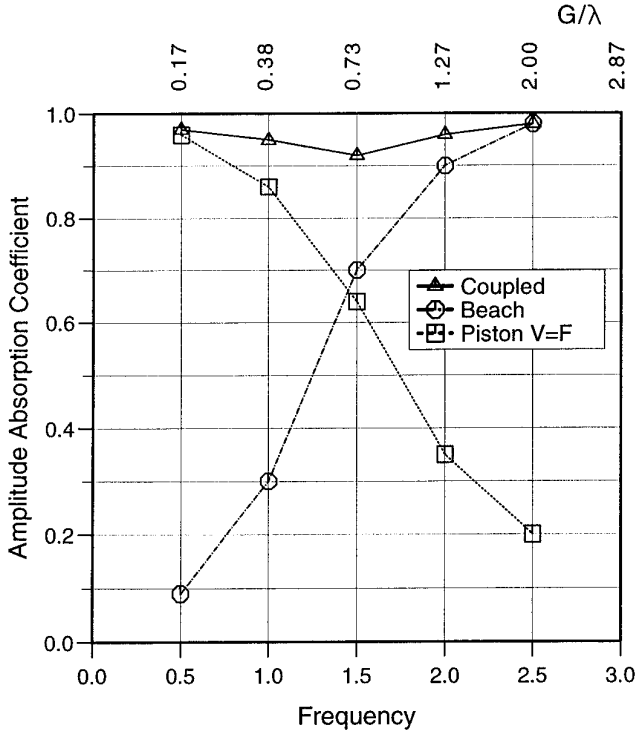

FIG. 8. Coupled Piston + Beach methods implemented in the *nonlinear* IBVP solver.

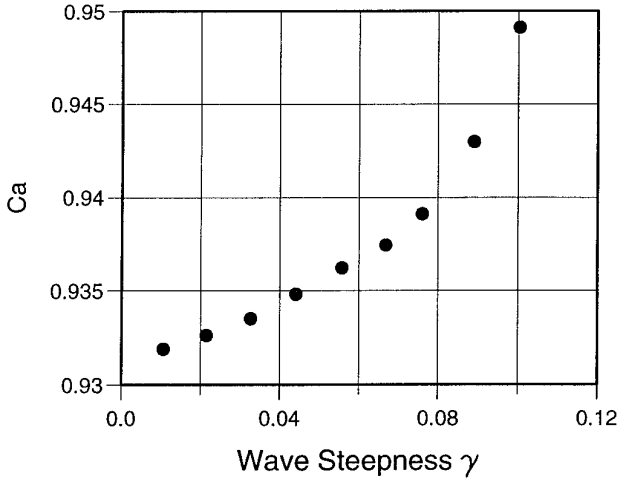

FIG. 9. Amplitude absorption coefficient versus wave steepness; normalized frequency $\omega(h/g)^{1/2} = 1.5$; normalized wavelength $\lambda/h = 2.73$.

TABLE I

Amplitude Absorption Coefficient C_A for Monochromatic (Diagonal) and Bichromatic Incident Wave Train

ω_1/ω_2	0.5	1.0	1.5	2.0	2.5	3.0
0.5	0.9512	0.9448	0.9360	0.9511	0.9673	0.9711
1.0		0.9402	0.9295	0.9353	0.9563	0.9684
1.5			0.9297	0.9409	0.9487	0.9648
2.0				0.9510	0.9554	0.9592
2.5					0.9721	0.9710
3.0						0.9749

Note. These coefficients were obtained using the linear code and the energy decay method via (2, 10).

We began our tests with bichromatic waves. They were generated by combining two monochromatic wave packets of frequencies ω_1, ω_2, separated by a time delay. This time lag was precomputed from the knowledge of the two group velocities and the basin length in such a way that the two waves arrive in the damping area at the same time (see Fig. 10). On Figs. 10 to 15, the lines show the free surface of the wave basin at successive time steps: the vertical axis is the time axis; the left edge is the wavemaker; the right edge is the wave-absorber.

Figure 10 shows such a waterfall view of the free surface during the simulation of a nonlinear bichromatic wave train with $\omega_1 = 0.5$, and $\omega_2 = 2.0$. Two thousand constant time steps ($\delta t = 0.1$) were necessary in this case, and only one curve every eight steps was plotted for the sake of legibility. The displacement of the wavemaker on the left edge and of the piston wave-absorber on the right edge of the figure can be observed, due to the fact that the computational domain evolves during nonlinear simulations. One can see the combination of short and long waves near the right end of the domain, and only the weak reflection after they have passed through the damping zone.

A systematic study with ω_1, ω_2 varying in the range of interest [0., 3.0] was achieved, using the coupling method

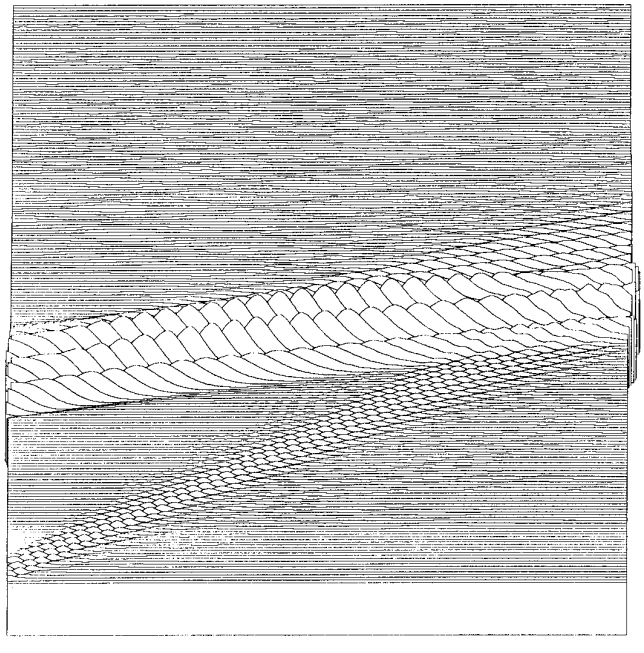

FIG. 10. Absorption of a nonlinear bichromatic wave train; $\omega_1 = 0.5$; $\omega_2 = 2.0$; $L = 36$.

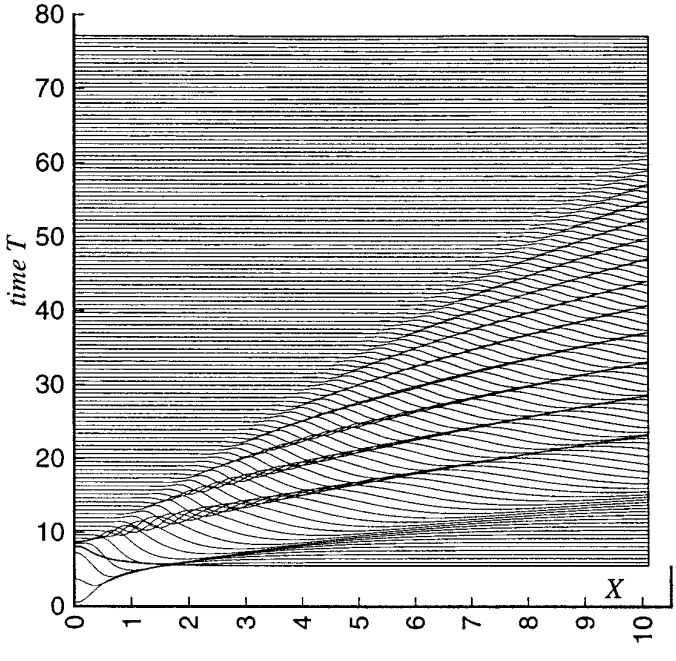

FIG. 11. Impulsive wavemaker motion; linear simulation. The *open boundary* reference solution.

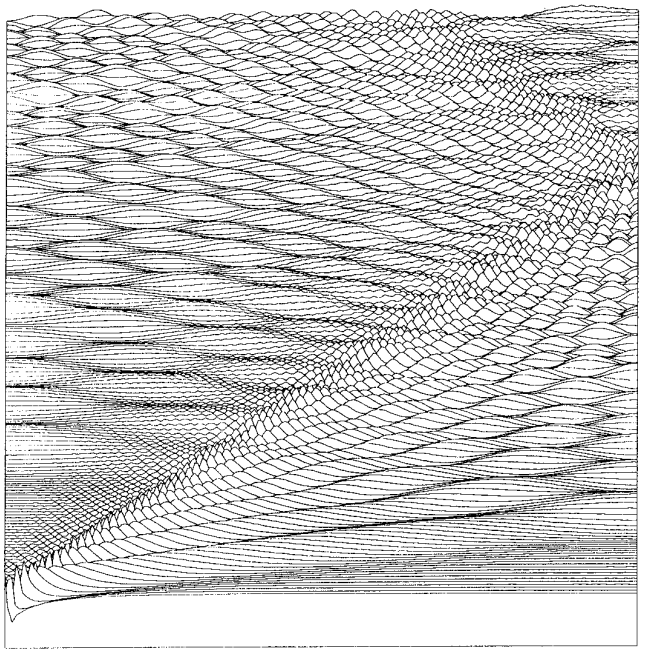

FIG. 12. Impulsive wavemaker motion; steady opposite wall; linear simulation.

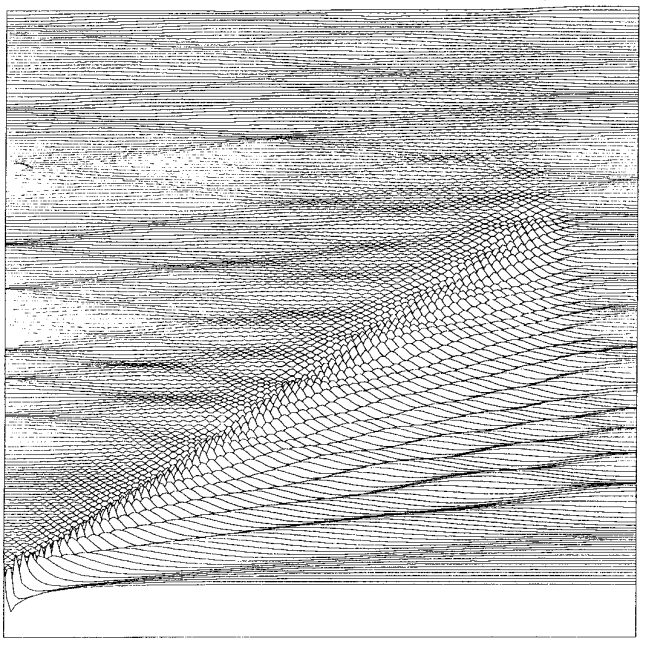

FIG. 14. Impulsive wavemaker motion; absorbing beach; $G = 2$; $L = 10$; linear simulation.

in the linear version of the code; The numerical results (see Table I) confirm the excellent results, even for the combination of very long waves with short ones (C_A (0.5, 3.0) = 0.9711), and they locate the overall minimum efficiency around $\omega_1 = 1.5$.

4.3. *Absorption of a Broad Bandwidth Spectrum*

In order to illustrate the independence of the method with regard to the spectral content of the incident wave train and its ability to work in situations actually unsteady

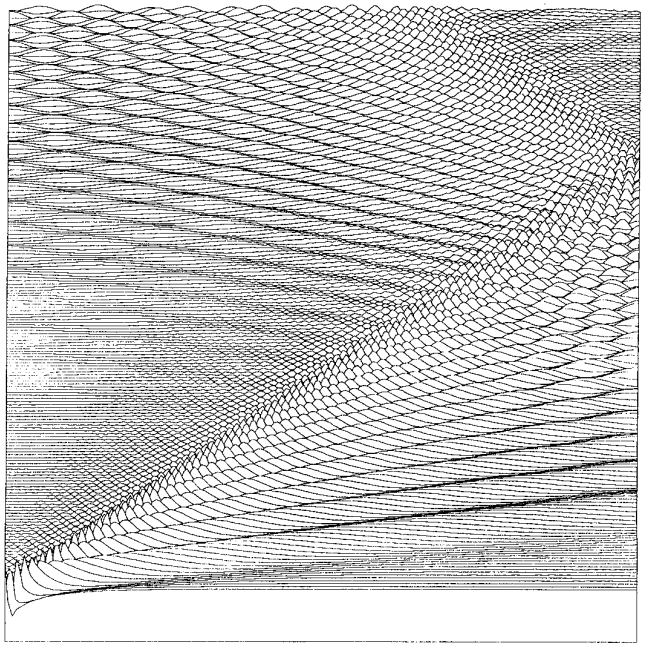

FIG. 13. Impulsive wavemaker motion; piston-like boundary condition $L = 10$; linear simulation.

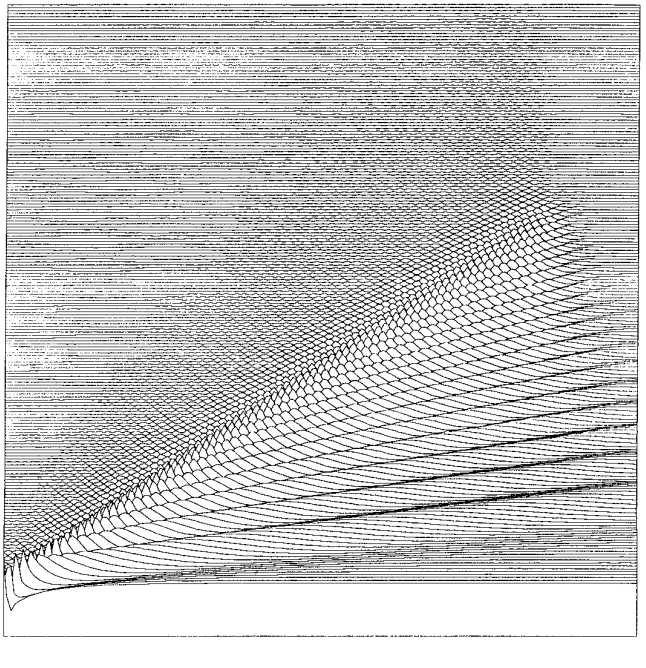

FIG. 15. Impulsive wavemaker motion; coupled piston + beach; $G = 2$; $L = 10$; linear simulation.

or transient, we subjected it to a very severe test case. At $t = 0$, the piston wave making surface $\mathscr{C}$ is given an impulsive velocity, $w(t) = \delta(t)$, in such a way that the incident wave train frequency at the opposite end $\mathscr{P}$ varies continuously, from the lower frequencies to the higher ones as time goes. This is due to the fact that the Fourier transform of the Dirac distribution is a constant so that all the frequencies are initially present in the spectrum and that, moreover, the wave group velocity is a function of the frequency which is the origin of the rays spreading in the (X, T) plane (Fig. 11); this particular behaviour resulting from the dispersive nature of the free surface condition is typical of unsteady free-surface hydrodynamics.

The computations reported in this section were performed with the linear code, but the corresponding nonlinear results (in [36]) show only slight differences with the present ones and lead to the same conclusions.

We first proceeded to the simulation in a long domain ($L = 30$) with the coupling method used at the output end in order to get reference results in the shorter range $0 < X < L = 10$ which will be used later, as if the basin were semi-infinite. This *open boundary* case is illustrated by Fig. 11 which shows what should happen if a perfectly absorbing condition (i.e., $C_A = 1.0$) was applied on $\mathscr{P}$.

Another interesting reference case was computed applying an homogeneous Neumann condition on $\mathscr{P}$ and no beach condition on the free surface, in order to simulate a perfectly reflecting wall (i.e., $C_A = 0$). On Fig. 12, one can observe the successive reflections of the initial system of diverging waves occurring upon, alternatively, the left and the right ends of the domain.

The three absorption strategies presented herein were tested in linear and then in nonlinear modelling: PABC alone; numerical beach alone; and coupled PABC + beach in a domain of length $L = 10$. Results of these three simulations in the linear case are given as a waterfall view on Figs. 13–15.

On Fig. 13, the PABC (2.7) was used on the right end of the basin. The high-pass character of this absorbing device is highlighted, by comparison with the reference simulations (Fig. 11–Fig. 12); the long leading waves are now cancelled while the shorter are partially and then completely reflected back in the computational fluid domain.

The simulation using the numerical beach alone as described in Section 3 is illustrated by Fig. 14, where now, the opposite low-pass filtering behaviour of this device may be observed.

Finally the very high damping of such a broad bandwidth incident wave spectrum obtained by coupling these two methods is clearly illustrated by Fig. 15.

5. CONCLUSION

A new simple strategy is proposed for the absorption of outgoing waves in linear and nonlinear numerical time-domain simulations of two-dimensional free-surface gravity waves. The basic idea lies in the coupling of two methods featuring complementary bandwidths. The first one, a Neumann boundary condition modelling a vertical piston driven by the hydrodynamic force acting upon its surface, is shown to be an asymptotically ideal long wave absorber (i.e., a *high-pass* water wave filter). The second one, a variant of the classical *numerical beach* device, gives its best in the small wavelength range (i.e., a *low-pass* water wave filter). The coupling of these methods is shown to be a very efficient damping strategy, with a 93% absorption coefficient in amplitude (99.5% in energy) in the worst case ($\omega \approx 1.5$). Thus, it seems to give better results than any other previous one (Orlanski, beach alone, piston alone) for the absorption of water waves of unknown frequency in the time-domain.

Moreover, the two following major advantages of the method must be emphasized:

It is straightforward to implement in linear and nonlinear solvers of water waves propagation problems, especially those based on BEM, and it gives as good results in the former case as in the latter one.

It does not require any kind of tuning, neither of the beach length nor of the Rayleigh dissipative term. This latter feature is very important, referring to the numerical consequences of using the beach alone, as numerous authors do. When doing so, the beach length must be increased proportionally to the longest wavelength supposed to be absorbed in order to maintain a good overall efficiency (see Fig. 6); this necessarily results in an increased number of unknowns (vertices, panels) and a heavier computational burden. This point, already sensitive in such 2D computations, will take on crucial importance in future simulations of 3D nonlinear free surface flows [39]. The present method does not behave so because the beach length is not linked to the longest waves to absorb; this work is done by the PABC.

ACKNOWLEDGMENT

I thank J. F. Domgin for his valuable help, especially in computer programming this method during his training stay in our laboratory, with the support of the French Ministry of Defense DRET.

REFERENCES

1. M. S. Longuet-Higgins and F. R. S. Cokelet, *Proc. R. Soc. London A* **350,** 1 (1976).
2. D. Givoli, *J. Comput. Phys.* **94,** 1 (1991).
3. J. B. Keller and D. Givoli, *J. Comput. Phys.* **82,** 72 (1989).
4. M. Johnsen, K. D. Paulsen, and F. E. Werner, *Int. J. Numer. Methods Fluids* **12,** 765 (1991).

5. D. Givoli, *Comput. Methods Appl. Mech. Eng.* **95,** 97 (1992).
6. B. Engquist and A. Majda, *Math. Comput.* **31**(139), 629 (1977).
7. A. Bayliss and E. Turkel, *Commun. Pure Appl. Math.* **32,** 707 (1980).
8. A. Barry, J. Bielak, and R. C. MacCamy, *J. Comput. Phys.* **79,** 449 (1988).
9. J. G. Blashak and G. A. Kriegsmann, *J. Comput. Phys.* **77,** 109 (1988).
10. A. Bayliss, M. Gunzburger, and E. Turkel, *SIAM J. Appl. Math.* **42**(2), 430 (1982).
11. W. M. Lin, J. N. Newman, and D. K. P. Yue, ''Nonlinear Forced Motions of Floating Bodies,'' in *Proceedings, 15th ONR Symp., Hamburg, 1984*.
12. A. Nestegard and P. D. Sclavounos, *J. Ship Res.* **28,** 48 (1984).
13. D. G. Dommermuth and D. K. P. Yue, *J. Fluid Mech.* **178,** 195 (1987).
14. J. V. Wehausen and E. V. Laitone, ''Surface Waves,'' in *Handbuch der Physik* (Springer-Verlag, New York/Berlin, 1960).
15. J. E. Romate, *J. Comput. Phys.* **99,** 135 (1992).
16. I. Orlanski, *J. Comput. Phys.* **21,** 251 (1976).
17. J. F. Lee and J. W. Leonard, *Ocean Eng.* **14**(6), 469 (1987).
18. S. Jagannathan, *Int. J. Numer. Methods Fluids.* **8,** 1051 (1988).
19. M. Brorsen, *Coastal Eng.* **11,** 93 (1987).
20. W. R. McCreight, ''Reflection Coefficients due to Open Boundary Conditions,'' *4th Int. Workshop Water Waves and Floating Bodies, Oystese, Norway, 1989*.
21. M. Israeli and S. A. Orszag, *J. Comput. Phys.* **41,** 115 (1981).
22. G. R. Baker, D. I. Meiron, and S. A. Orzag, *J. Fluid Mech.* **123,** 477 (1982).
23. R. Cointe, *Thèse de l'Ecole Nationale des Ponts et Chaussées,* Paris, 1989 (unpublished).
24. R. Cointe, ''Nonlinear Simulation of Transient Free Surface Flows,'' in *Proceedings, 5th Int. Conf. Num. Ship Hydrodynamics, Hiroshima, Japan, Sept. 1989*.
25. A. Clément and C. Maisondieu, ''Comparison of Time-Domain Control Laws for a Piston Wave Absorber,'' in *Proceedings, European Wave Energy Symposium, Edinburgh, Scotland, July 1993,* edited by G. Elliot and G. Caratti (NEL, East Kilbride, Scotland, 1994), p. 117.
26. C. Maisondieu, *Thèse Universté de Nantes, France,* 1993 (unpublished).
27. A. Clément, ''Exemples de simulations d'écoulements instationnaires non-linéaires à surface libre par la méthode mixte Euler–Lagrange,'' in *Proceedings, 3èmes Journées de l'Hydrodynamique, Grenoble, France, 1991*.
28. N. D. Hasley, *Ph.D. thesis. California State University, Long Beach,* 1977 (unpublished).
29. D. Sen, J. S. Pawlowski, J. Lever, and M. J. Hinchey, ''Two-Dimensional Numerical Modelling of Large Motions of Floating Bodies in Waves,'' in *Proceedings, 5th Int. Conf. Num. Ship Hydrodynamics, Hiroshima, Japan, 1989*.
30. D. Sen, *J. Ship Res.* **37**(4), 307 (1993).
31. T. Vinge and P. Brevig, ''Nonlinear Ship Motions, in *Proceedings, 3rd Int. Conf. Numer. Ship Hydrodyn, Paris, France, 1981*.
32. J. Milgram, *J. Fluid Mech.* **43**(4), 845 (1970).
33. S. Naito and S. Nakamura, *Hydrodynamics of Ocean Wave-Energy Utilization* (Springer-Verlag, New York/Berlin, 1985), p. 269.
34. Y. Cao, R. F. Beck, and W. W. Schultz, ''An Absorbing Beach for Numerical Simulations of Nonlinear Waves in a Wave Tank,'' in *Proceedings, 8th Int. Workshop Water Waves and Floating Bodies, St. John's, Newfoundland, Canada, 1993.*
35. J. G. Telste, *J. Fluid. Mech.* **182,** 149 (1987).
36. A. Clément and J. F. Domgin, *J. Estudos de Engenharia Civil* **6,** 257 (1994).
37. R. W. Yeung and M. Vaidhyanathan, *Int. J. Numer. Methods Fluids* **14,** 1111 (1992).
38. M. Isaacson and K. F. Cheung, *Appl. Ocean Res.* **13**(4), 175 (1991).
39. P. Ferrant, ''Radiation and Diffraction of Nonlinear Waves in Three Dimensions,'' in *Proceedings, 7th Int. Conf. Behaviour Offshore Structures BOSS'94, Boston, 1994* (Pergamon, Elmsford, NY, 1994).